https://doi.org/10.5194/egusphere-2025-3884
Preprint. Discussion started: 21 August 2025


# Improving Snow Simulations through Improved Representations of Vegetation Conditions: Insights from High Resolution Simulations over California

Aniket Gupta[1], Ali Behrangi[1], Mohammad Farmani[1], Patrick Broxton[2], Guo-Yue Niu[1]

[1]Department of Hydrology and Atmospheric Sciences, The University of Arizona, Tucson, AZ, United States
[2]School of Natural Resources and the Environment, The University of Arizona, Tucson, AZ, United States

*Correspondence to*: Aniket Gupta (aniketgupta@arizona.edu) and Guo-Yue Niu (niug@arizona.edu)

**Abstract.** Most hydrological models underestimate snow water equivalent (SWE) in the mountainous western US. Key limitations may be due to coarse resolution precipitation input and inadequate representations of snow-vegetation interactions. Vegetation affects snow dynamics through snow interception, throughfall/unloading, and energy transfer through the canopy, yet basin-scale studies on the vegetation effects are limited. To address this issue, we applied the Noah-MP version 5.0 with a dynamic vegetation module to the Sacramento and San Joaquin River Basins in California at 1 km resolution driven by forcing from Analysis of Record for Calibration (AORC) and NLDAS-2, downscaled to 1 km using the WRF-Hydro Meteorological Forcing Engine. We carried out eight model experiments driven by the two forcing datasets and two vegetation schemes over the two Basins. Compared to 4 km PRISM and 1km AORC, the downscaled 1 km NLDAS-2 forcing data shows higher precipitation and lower temperatures over the mountains, resulting in more snowfall and SWE, which is more consistent with in-situ SWE observations. Using the 1-km NLDAS-2 forcing, the default vegetation scheme with prescribed leaf area index (LAI) and vegetation cover fraction produces too much SWE on the ground due mainly to the strong canopy shading effect despite more snow intercepted by the canopy. The dynamic vegetation module produces smaller LAI than the prescribed (more consistent with MODIS data) and thus leads to more shortwave radiation reaching the snow surface, thereby enhancing episodic melting during the accumulation season. Validation against in-situ snow data suggests that the use of dynamic vegetation model and the downscaled NLDAS-2 data performs the best. These findings highlight the importance of vegetation effects and downscaling of atmospheric forcing to increase the accuracy of snow modeling over the Southwest US.

**Keywords:** Snow modeling; vegetation effects; atmospheric downscaling; snow interception; Noah-MP

**Plain language summary.** Most hydrological models tend to underestimate snow over the southwest US mountains. This includes inaccurate precipitation input and/or inadequate representations of snow-vegetation interactions that strongly affect snow accumulation/melt due to the important but counteracting effects of interception and shading of the vegetation canopy. Through model experiments, we show the importance of downscaling and vegetation shading effects to improve the accuracy of snow modeling over the southwest US.

https://doi.org/10.5194/egusphere-2025-3884
Preprint. Discussion started: 21 August 2025


**Key highlights:**

- Downscaled NLDAS-2 atmospheric forcing data produces more precipitation than AORC and PRISM forcing, resulting in more snow.
- Canopy shading effects on snowmelt/sublimation are more important than canopy interception effects on snow beneath the canopy.
- The use of a dynamic vegetation model, which produces more accurate LAI, and downscaled NLDAS-2 data improves snow simulation.

## 1 Introduction

Snow Water Equivalent (SWE) is important in regions like California where snowpack plays a vital role in freshwater supply and management. Studies show that mountain snowpack contributes to 70-80% of the total annual runoff yield in the western United States (Daly et al., 2000b; Li et al., 2017). With complex terrain and a Mediterranean climate, California experiences significant variability in precipitation amount and patterns, which affect snowpack in the Sierra Nevada mountains. Snow dynamics are impacted by multiple factors such as precipitation, temperature, topography, wind, and vegetation (Anderson et al., 2014; Mott et al., 2018). Despite significant advancements, most hydrological models produce less SWE in the Southwest US than is observed (Cho et al., 2022; Garousi-Nejad and Tarboton, 2022; Fang et al., 2022). Various global reanalyses like ERA, ERA-Land, MERRA-2 and GLDAS significantly underestimate SWE in the Southwest US due to their coarse resolution, deficiencies in model physics (e.g. melting processes) and lack of SWE data assimilation (Broxton, 2016). Furthermore, most land surface models (LSMs) produce less SWE even with advanced snow physics and complex radiation transfer schemes due to inaccurate atmospheric forcing data (Cho et al., 2022; Toure et al., 2016; Garousi-Nejad and Tarboton, 2022). For instance, the NCAR CLM v4.0, driven by the MERRA atmospheric forcing data, produces only a small portion (~20%) of the SNOTEL SWE (Toure et al., 2016). Noah-MP (Niu et al., 2011) used in the National Water Model (NWM) (at 1-km resolution) produces a better match with the SNOTEL data but still underestimates SWE by 20% – 30% (Cho et al., 2022; Garousi-Nejad and Tarboton, 2022).

The interactions between snow and vegetation represents a critical component of SWE dynamics impacting hydrology, biodiversity, and ecosystem services. With diverse landscapes ranging from the coastal forests to the alpine meadows, California exhibits a complex interplay between snowpack accumulation and vegetation distribution. Understanding the interactions are essential for predicting and managing water resources, drought, flood, serving biodiversity, and mitigating the impacts of climate change on ecosystems. Snow cover and vegetation work in a feedback manner and play a significant role in ecosystem productivity across varying landscapes (Cook et al., 2008; Euskirchen et al., 2016). In the mountainous regions such as the Sierra Nevada, snow accumulation during the winter months serves as a primary water source for vegetation growth during the dry summer and helps sustain vegetation through prolonged droughts. The timing and duration of snowmelt

https://doi.org/10.5194/egusphere-2025-3884
Preprint. Discussion started: 21 August 2025




influence the onset of plant growth, with earlier snowmelt generally leading to earlier vegetation green-up and extended growing seasons (Cooper et al., 2011; Livensperger et al., 2016). Vegetation, in turn, influences snow accumulation and melting processes through various biophysical feedback mechanisms. Forests, for example, can modify snowpack characteristics by reducing the wind speed, intercepting snowfall, altering snowpack density, and reducing surface albedo through canopy shading (Niu and Yang, 2004; Bartlett and Verseghy, 2015; Stähli et al., 2009). Shrubs and grasses in montane and subalpine ecosystems can also affect snow distribution by trapping snow in the winter and shading the snow surface in the spring, thus influencing the timing and magnitude of snowmelt runoff.

Studies examining the interactions between snow and vegetation range from advanced field observations to remote sensing and distributed modeling approaches. Field studies include (but are not limited to) measuring snow depth, density, sap flow, leaf area index (LAI), normalized difference vegetation index (NDVI), nutrient storage and transport, vegetation characteristics at various sites across different elevational gradients (Hwang et al., 2009; O'Keefe et al., 2020; Rey et al., 2021). Remote sensing techniques provide valuable tools for assessing snow-vegetation interactions over larger spatial scales. Satellite-based sensors, such as those aboard NASA's Landsat, MODIS and Copernicus's Sentinel missions, and airborne LiDAR offer insights into snow cover extent, vegetation phenology, and land surface properties. By analyzing SWE and vegetation greenness data, researchers can quantify snow-vegetation relationships and monitor growing season, peak photosynthesis to facilitate development of more realistic carbon cycle representations in models (Tennant et al., 2017; Wang et al., 2018). Numerical modeling approaches, including coupled snow-vegetation models, facilitate the integration of biophysical processes governing snow dynamics and vegetation responses (e.g., Niu and Yang, 2004). These models simulate snow accumulation, melt, and redistribution in conjunction with vegetation growth, productivity, and water use. By incorporating ecological parameters such as plant phenology, leaf area index, and root water uptake, these models provide insights into the complex feedback between snow and vegetation in regional ecosystems (Bonan et al., 2003; Franklin et al., 2020).

Modeling approaches to understand the interactions between snow and vegetation plays a crucial role in elucidating the complex dynamics of these two key components of the ecosystems. Numerical models serve as powerful tools for predictive understanding of the coupled processes governing snow accumulation, melt, and redistribution, as well as vegetation growth, productivity, and water use. By integrating physical, biological, and ecological processes, these models enable researchers to explore the feedback and interactions between snow and vegetation across different spatial and temporal scales. One prominent modeling approach used in studying snow-vegetation interactions is the use of land surface models (LSMs). LSMs simulate the exchange of energy, water, carbon, and momentum between the land surface and the atmosphere, incorporating processes such as snow accumulation, melt, and sublimation, as well as vegetation dynamics (Overgaard et al., 2006). Noah-MP is one of the state-of-the-art LSM that simulates the complex snow-vegetation interactions through the dynamic leaf model and snow evolution scheme (Niu et al., 2004). The snow model of Noah-MP represents one of the best snow models compared to other LSMs like JULES, Catchment LSM, and Noah (Cho et al., 2022). However, compared to SNOTEL measurements of annual

https://doi.org/10.5194/egusphere-2025-3884
Preprint. Discussion started: 21 August 2025


maximum SWE, Noah-MP tends to underestimate SWE depending on elevation ranges, and the higher elevation the larger underestimation of SWE partially due to low snowfall estimates (Cho et al., 2022).

This study aims to 1) improve the modelling accuracy of SWE through improved estimates of precipitation at a high resolution and the use of a dynamic vegetation model and 2) improve the understanding of the impacts of vegetation interception/sublimation and shading/scattering of radiation on snowpack accumulation and ablation. We use Noah-MP version 5 with a dynamic vegetation model to predict LAI and green vegetation fraction to explore the vegetation effects on snowpack simulation at a high resolution.

## 2 Study Area

The Noah-MP model was set up over two HUC-4 basins in California: the Sacramento and San Joaquin Rivers (Fig. 1). The Sacramento River Basin covers ~70,000 km$^2$ in northern California and includes significant snow cover and forests in the southern Cascade Mountains, Klamath Mountains and Sierra Nevada (Domagalski, 1998). The San Joaquin River Basin covers an approximate area of 40,000 km$^2$ in central California. The 483 km long river originates in the Sierra Nevada mountains and meets the Sacramento River along its north-east border. Snowmelt runoff from the mountains is the main source of freshwater in the San Joaquin and Sacramento River Basins (Brekke et al., 2004). These two basins differ in their altitude and vegetation cover which can potentially impact the snow-vegetation interaction.

https://doi.org/10.5194/egusphere-2025-3884
Preprint. Discussion started: 21 August 2025


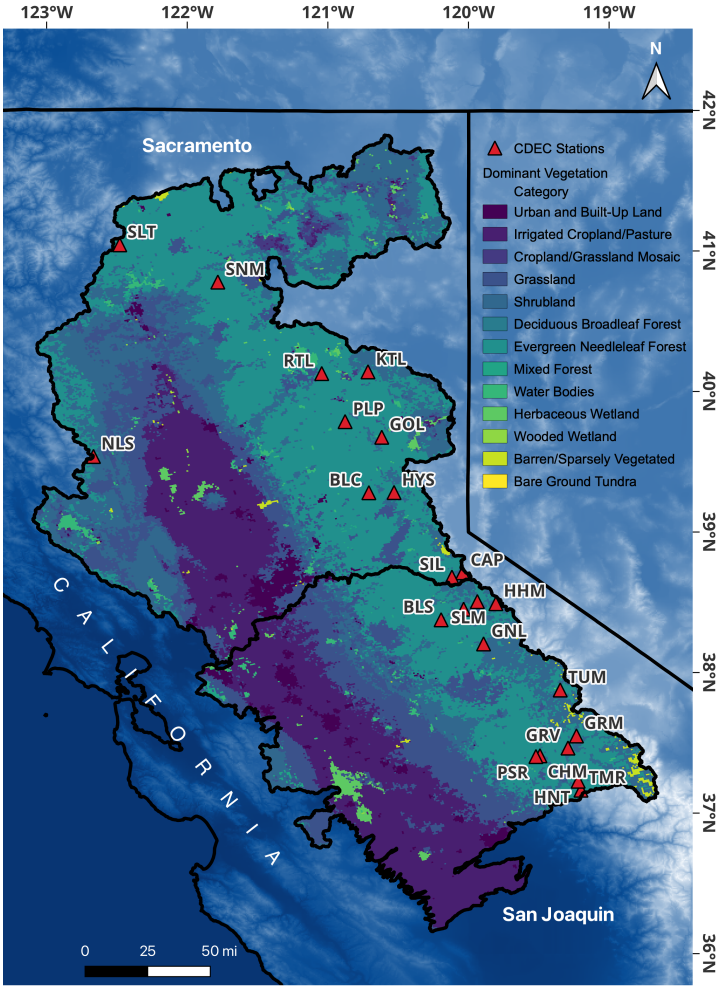


**Figure 1.** Study Area representing the Sacramento and San Joaquin Basins (HUC4) in California with dominant vegetation types. The red triangles represent the Snow Water Equivalent (SWE) stations of the California Data Exchange Center (CDEC).

110

https://doi.org/10.5194/egusphere-2025-3884
Preprint. Discussion started: 21 August 2025


## 3 Data

### 3.1 Forcing Data

We used two gridded meteorological forcing datasets including the Analysis of Record for Calibration (AORC) and the North American Land Data Assimilation System (NLDAS-2). AORC version 1.1 was developed at National Weather Service as a part of development of the CONUS scale hydrologic modeling capability and establishment of the National Water Model (Kitzmiller et al., 2018). AORC is a meteorological forcing dataset at 1 km spatial resolution and hourly temporal resolution over CONUS region and provides 8 variables required to drive hydrological or land surface models. AORC data has been developed using the multiple sources which includes NLDAS-2, LIV16, NEXRAD Stage IV, URMA, and a climatology from PRISM (Greg Fall et al. 2023, JAWRA) over the NWM grid. AORC v1.1 is available from 1979 – 2023 as part of version 3 of the National Water Model (NWM). NLDAS-2 is a primary forcing file for Phase 2 of the North American Land Data Assimilation System (NLDAS). The datasets are available at 1/8th-degree and hourly temporal resolution. It combines multiple observational data from gauge, satellite, and radar to produce the time series of meteorological variables (Xia et al., 2012). It extends from January 1979 to present over North America. We further downscaled this dataset to 1 km spatial resolution to match the AORC grids (see section 4.2).

### 3.2 Validation data

#### 3.2.1 PRISM

We used PRISM (Parameter-elevation Regressions on Independent Slopes Model) daily data to evaluate precipitation and temperature from AORC and the downscaled NLDAS-2 data. PRISM, which is developed and maintained by the PRISM Climate Group at Oregon State University, provides high-resolution (4 km) daily climate data for various meteorological variables (Daly et al., 2000a). Monthly normals are the baseline datasets which are modeled using digital elevation model as a predictor grid and the daily normals are derived using the "nudging and smoothing" technique. The daily normals include precipitation, minimum, maximum & mean temperature, and minimum & maximum vapor pressure deficit over the CONUS. In this study we have used the daily temporal resolution temperature and precipitation datasets from PRISM. Note that all 1 km datasets (AORC and downscaled NLDAS data) are averaged to 4 km resolution for the comparison.

#### 3.2.2 NWM 3.0 SWE

To analyze the improvement in snow estimation with respect to current operational NWM we have downloaded 5-year (2015 – 2019) retrospective SWE estimation from NWM v3.0. NWM uses the prescribed monthly LAI, the Jordan (1991) scheme for rain-snow partitioning, the Ball-Berry scheme for stomatal resistance and the BATS scheme (Dickinson et al., 1993) for snow surface albedo. The retrospective simulations from NWM v3.0 are available for a period between 1979 – 2023 and can

https://doi.org/10.5194/egusphere-2025-3884
Preprint. Discussion started: 21 August 2025


be downloaded from the Amazon Web Service (AWS) storage (https://registry.opendata.aws/nwm-archive/). These datasets are available at 3-hourly, which we aggregated to daily timescale for daily comparison.

#### 3.2.3 UA-SWE

UA snowpack data (UA-SWE), developed at the University of Arizona, is based on observed SWE and snow depth from Snow Telemetry (SNOTEL) and National Weather Service Cooperative Observer stations across CONUS (Broxton et al., 2024). Initially, UA-SWE was developed at 4 km daily resolution using the 4 km PRISM data, though they have recently been downscaled to 800 m resolution by using 800 m PRISM climate data, and accounting for the effects of smaller-scale topographic and forest cover variations (Broxton et al 2023). Generally, the 800 m and 4 km versions are similar, except the 800 m version shows more detail and has a little less SWE in forested areas. This study uses the 800 m version of the UA-SWE dataset.

#### 3.2.4 SNODAS

Snow Data Assimilation System (SNODAS) is a data assimilation system developed by National Operational Hydrologic Remote Sensing Center (NOHRSC) at NOAA (Barrett, 2003). SNODAS provides snow cover estimates at 1 km and daily resolution to support the hydrological modeling and analysis. SNODAS assimilates data from satellite, airborne platforms, and ground stations. The main inputs to the SNODAS includes the downscaled outputs from numerical weather prediction (NWP) models to simulate the snow cover using a physically based, mass and energy balance snow model.

#### 3.2.5 MODIS and SUN YAT-SEN LAI

This study uses the MOD15A2H Version 6.1 data from the Moderate Resolution Imaging Spectroradiometer (MODIS) sensor on-board the Terra satellite. MODIS captures data in 36 spectral bands (Myneni et al., 2021) and provides detailed information about the Earth's surface and atmosphere, including vegetation, land cover, and cloud properties. The MOD15A2H dataset is a combined LAI and Fraction of Photosynthetically Active Radiation (FPAR) product that is an 8-day composite with 500-meter spatial resolution. In this study, we aggregate the 8-day product into seasonal data for comparison with the modelled data. We also used the reprocessed MODIS Version 6.1 LAI data from Land-Atmospheric Interaction Research Group at Sun Yat-Sen University (Lin et al., 2023). Their product applies spatio-temporal filtering and smoothing to MODIS LAI data to reduce their spatial and temporal inconsistency. These datasets are also available at the 8-day temporal resolution and 500-meter spatial resolution which have been converted to seasonal data for comparison in this study.

https://doi.org/10.5194/egusphere-2025-3884
Preprint. Discussion started: 21 August 2025


### 3.2.6 CDWR stations

California Cooperative Snow Surveys (CCSS), which is part of the California Department of Water Resources (CDWR), conducts snow surveys in the mountains of California (https://water.ca.gov/Programs/Flood-Management/Flood-Data/Snow-Surveys). Established in 1929 by the California Legislature, this program is a partnership of more than 50 state, federal, and private agencies. CCSS maintains a total of 265 snow courses and 130 snow sensors located throughout the Sierra Nevada and Shasta-Trinity mountains. This study uses data from 23 CDWR stations across the study area to obtain the precipitation, temperature and SWE data (Fig. 1).

## 4 Methods

### 4.1 Noah-MP version 5

Noah-MP was developed as a community effort to improve the Noah Land Surface Model (LSM) by adding a vegetation canopy layer and incorporating multiple physics options to parametrize different land-surface processes (Niu et al., 2011; Yang et al., 2011; He et al., 2023). Recently Noah-MP has been upgraded to a modularized version, Noah-MP Version 5.0, which represents each process with one separate module (He et al., 2023). Noah-MP is a grid based columnar model, which calculates the precipitation partitioning into surface and subsurface fluxes through physical equations, while preserving the energy and mass balance at each time step. Biogeophysical and biogeochemical processes are separately calculated for different land use classes, which are based on USGS or MODIS land type data. Major processes include canopy interception, canopy evaporation/sublimation, snow accumulation, snowpack evaporation/sublimation, snowmelt, soil surface evaporation, transpiration, infiltration, surface runoff, and subsurface runoff. The infiltrated water moves further through the soil column following the Richard's equation in the vadose zone. Finally, the water leaving the bottom of the soil column is considered as groundwater recharge in Noah-MP.

The snow component in Noah-MP is a process-based, multi-layer, and multi-physics energy balance model. Its layered design enables the simulation of internal snowpack dynamics such as compaction, water storage, and refreezing. A thin surface layer is included to better capture turbulent energy exchanges, which, together with net radiation, represent the primary energy to the snow layer that control snowpack temperature and the energy available for melt (Niu et al., 2011). The model also considers the energy required to change a snow layer to the melting/freezing points as well as the latent heat involved in phase changes between liquid water and ice. The model also accounts for temporally variable snow surface albedo (Wang et al., 2000), vegetation shading/scattering of radiation (Niu & Yang, 2004), and fractional snow cover (Niu & Yang, 2007).

https://doi.org/10.5194/egusphere-2025-3884
Preprint. Discussion started: 21 August 2025


#### 4.1.1 The Snow Interception Model in Noah-MP

The snow interception model of Noah-MP represents the mass balance of the ice and liquid water on the canopy. It represents loading and unloading of snowfall, interception of rainfall and dripping of the intercepted water, sublimation/evaporation of the ice/liquid water on the canopy, melt of the intercepted snow and freezing of the melt water and intercepted rain (Niu et al., 2004). Following Hedstrom and Pomeroy (1998), Noah-MP represents the snow interception rate (or loading rate) as

$$Q_{ice,intcp} = (W_{ice,max} - W_{ice})\left(1 - e^{-P_{snow}\Delta t/W_{ice,max}}\right), \quad (1)$$

where $\Delta t$ is the time step, and $P_{snow}$ (kg m$^2$ s$^{-1}$), W$_{ice}$, and $W_{ice,max}$ (kg m$^{-2}$) are the snowfall rate, the canopy-intercepted snow, and the maximum canopy load for snow, respectively. $W_{ice,max}$ adopts the scheme of Schmidt and Gluns (1991):

$$W_{ice,max} = 6.6 \times \left(2.7 + \frac{46}{\rho_{snowfall}}\right) \times (E_{LAI} + E_{SAI}), \quad (2)$$

where $\rho_{snowfall}$ is the bulk snowfall density [kg/m$^3$], which is represented as a function of surface air temperature, $E_{LAI}$ and $E_{SAI}$ are the effective leaf area index [m$^2$/m$^2$] and the effective stem area index [m$^2$/m$^2$], respectively, both of which are not buried by snow. Assuming $\rho_{snowfall}$ = 100 kg/m$^3$, $W_{ice,max}$ is ~50 times the maximum load for liquid water.

The snowfall rate below the canopy, $Q_{snow}$ [mm/s], is

$$Q_{snow} = \left(1 - F_{veg}\right) \times P_{snow} + Q_{ice,drop}, \quad (3)$$

where the first term on the right hand-side represents canopy throughfall, and $F_{veg}$ is the vegetation cover fraction. The rate of snow drops from the vegetated fraction, $Q_{ice,drop}$ [mm/s] is updated as

$$Q_{ice,drop} = \left(F_{veg} \times P_{snow} - Q_{ice,intcp}\right) + Q_{ice,unload}, \quad (4)$$

where the first term in the right hand-side represents the snowfall that is unable to be intercepted by the canopy, and $Q_{ice,unload}$ is the canopy snow unloading rate depending on the canopy temperature and wind speed (Roesch et al., 2001; Niu et al., 2004). Note that the snowpack on the ground also receives liquid water dripping from the canopy and throughfall of rain to represent rain-on-snow events.

https://doi.org/10.5194/egusphere-2025-3884
Preprint. Discussion started: 21 August 2025


#### 4.1.1 The Radiation Transfer Model in Noah-MP

Noah-MP represents the vegetation shading and scattering effects of shortwave radiation through a modified two-stream radiation-transfer approximation, which considers the probabilities of between-canopy and within-canopy gaps (Niu et al., 2004; Yang and Friedl 2003). It computes the below-canopy radiative fluxes that reach the snowpack on the ground including direct shortwave (including that is transmitted through the canopy gap) and diffuse shortwave (including direct and diffuse components that are scattered by the canopy and the diffuse component that is transmitted through the canopy gaps) and above-canopy upward fluxes per unit incident direct and diffuse shortwave (i.e., the surface albedo) over the visible and near-infra wavebands. The between- and within-canopy gaps are computed from the canopy geometry parameters including canopy thickness, crown radius, and tree density as well as LAI and SAI. The model also accounts for the longwave radiation received by the ground snow surface including the atmosphere longwave radiation that are not intercepted by the vegetation canopy and that emitted by the canopy; such impacts can be reduced or intensified based on LAI, SAI and tree density in a grid.

#### 4.1.2 The Dynamic Vegetation Module in Noah-MP

The dynamic vegetation model of Noah-MP is composed of two models which includes a plant physiology model and a phenology model. In Noah-MP, photosynthesis for C3 plants is simulated using the model of Farquhar et al. (1980), as modified by Collatz et al. (1991), while C4 plant photosynthesis follows Collatz et al. (1992). For C3 plants, the photosynthetic rate is determined by the minimum of three limiting processes: Rubisco activity, light availability, and the transport of photosynthetic products; for C4 plants, it is constrained by PEP-carboxylase activity. The model also incorporates a short-term phenology scheme that regulates how photosynthates are allocated to carbon pools in different plant components like leaf, stem, wood, and root. It can also simulate the plant degradation due to cold and drought stress, age decay, phytophagic activity, and physical damage (Dickinson et al., 1998). Leaf area index (LAI) and stem area index (SAI) are derived from leaf and stem carbon storage using specific leaf/stem area ($m^2\ gC^{-1}$), which vary by vegetation type (He et al., 2023; Niu et al., 2011). The vegetation greenness fraction (GVF) is computed as a function of the predicted LAI and SAI (Niu et al., 2011):

$$GVF = 1 - e^{0.52(LAI+SAI)} \quad (5)$$

### 4.2 Downscaling

The meteorological variables from NLDAS-2 at 1/8 degree have been downscaled to 1 km resolution using the WRF Hydro Meteorological Forcing Engine (MFE), which uses the statistical downscaling approach using the mountain mapper algorithm to improve the quantitative estimate of precipitation (QPE). Precipitation downscaling used a correction factor based on the ratio of gauge observed precipitation and the PRISM climatology. Temperature was downscaled using the National Center for Atmospheric Research (NCAR) lapse rate over the CONUS region. All other variables were downscaled using the topographic adjustment according to elevation (https://github.com/NCAR/WrfHydroForcing).

https://doi.org/10.5194/egusphere-2025-3884
Preprint. Discussion started: 21 August 2025


### 4.3. Domain discretization and model setup

Noah-MP v5 was set up for the Sacramento and San Joaquin basins at 1 km spatial and hourly temporal resolution using hourly AORC v1.1 and downscaled NLDAS-2 forcing data. The Sacramento River Basin domain has 363×310 (south-north, west-east) grids and the San Joaquin domain has a 285×252 (south-north, west-east) grids. The simulation period is between 2015 – 2019 (5 years), and the model was spun up for a period of 5 years. The model simulations were performed in Lambert Conformal Conic (LCC) projection consistent with the forcing data. The maximum soil depth was set to 2 meters with 4 layers while the snowpack had up to three layers depending on snow depth. We selected two dynamic vegetation options (Table 1) including different combinations of LAI and GVF options. The prescribed monthly LAI climatology is from a lookup table of LAI, which were prescribed for a specific vegetation type based on global mean values. The prescribed GVF is assumed as a maximum yearly vegetation fraction. Combining the two basins, two forcing datasets, and two dynamic vegetation options, a total of 8 simulations were carried out in the study. Other physics options used in the Noah-MP are summarized in Table 2.

**Table 1.** Simulation acronyms and dynamic vegetation options used in the study.

| ACRONYMS | DynVeg_Off | DynVeg_Pred |
|---|---|---|
| LAI | Prescribed monthly LAI climatology | Dynamic (predicted from carbon storage) |
| GVF | Prescribed yearly maximum GVF | Dynamic (predicted from LAI) |

**Table 2.** Noah-MP physics option used in the study related to snow-vegetation interaction.

| Noah-MP physics | Noah-MP options |
|---|---|
| Stomata Resistance (dynamic vegetation) | Ball-Berry scheme (Ball et al., 1987) |
| Rain-snow partitioning | Jordon (1991) |
| Snow layer temperature | Semi-implicit (Niu et al., 2011) |
| Snow albedo | BATS snow albedo (Dickinson et al., 1993) |
| Canopy radiation transfer | Two-stream (Dickinson et al., 1983) |
| Soil hydrology | Noah (Ek et al., 2003) |

https://doi.org/10.5194/egusphere-2025-3884
Preprint. Discussion started: 21 August 2025


## 5 Results

### 5.1 Meteorological Downscaling

The downscaled NLDAS-2 datasets in the spatial plots shows more precipitation compared to AORC however, the daily mean aligns well with PRISM observation (Fig. 2). Especially, in the higher altitude NLDAS-2 shows more precipitation compared to AORC. Precipitation intensity also is quite underestimated in AORC compared to PRISM and NLDAS-2 in both the basins. In the Sacramento River Basin, the average daily PRISM precipitation is 2.6 mm, and the downscaled NLDAS-2 precipitation shows the same magnitude (Fig. 2). However, AORC shows an underestimation of precipitation by a magnitude of 0.1 mm $day^{-1}$ averaged over the five-year period. More apparently, NLDAS-2 shows higher intensity precipitation especially over the Serra Nevada Mountain range (Fig. 2) than does the AORC forcing at higher elevations. Such discrepancies lead to underestimation of snow over the high mountains. Both AORC and NLDAS-2 precipitation data uses PRISM climatology as a reference; hence, their spatial precipitation patterns are quite similar. However, AORC underestimates the amount and intensity of precipitation when compared to PRISM and NLDAS-2 at high elevations. Elevation dependent boxplots show that AORC constantly underestimates the precipitation at all elevations, but particularly at the highest elevations (Fig. 2d). NLDAS-2 slightly underestimates the precipitation at lower elevations, however, it produces larger precipitation at high elevations where there is substantial snowfall. The precipitation from NLDAS-2 aligns quite well with PRISM between 1000 m to 3000 m (Fig. 2d), and this range also agrees with the mean precipitation from the available CDWR stations (represented with * in Fig. 2d, h), however the gauge undercatch, which is more serious for snowfall, is not corrected at these stations (as discussed later in the discussion section).

In the San Joaquin River Basin, NLDAS-2 also shows identical daily-mean precipitation (1.8 mm $day^{-1}$) as PRISM (Fig. 2e–g), while AORC shows a lower value (1.7 mm $day^{-1}$), ~0.1 mm $day^{-1}$ less. As in the Sacramento River Basin, downscaled NLDAS-2 and PRISM data also have similar spatial patterns (with comparable amounts), but AORC has too little precipitation in mountainous areas in the San Joaquin River Basin.

https://doi.org/10.5194/egusphere-2025-3884
Preprint. Discussion started: 21 August 2025


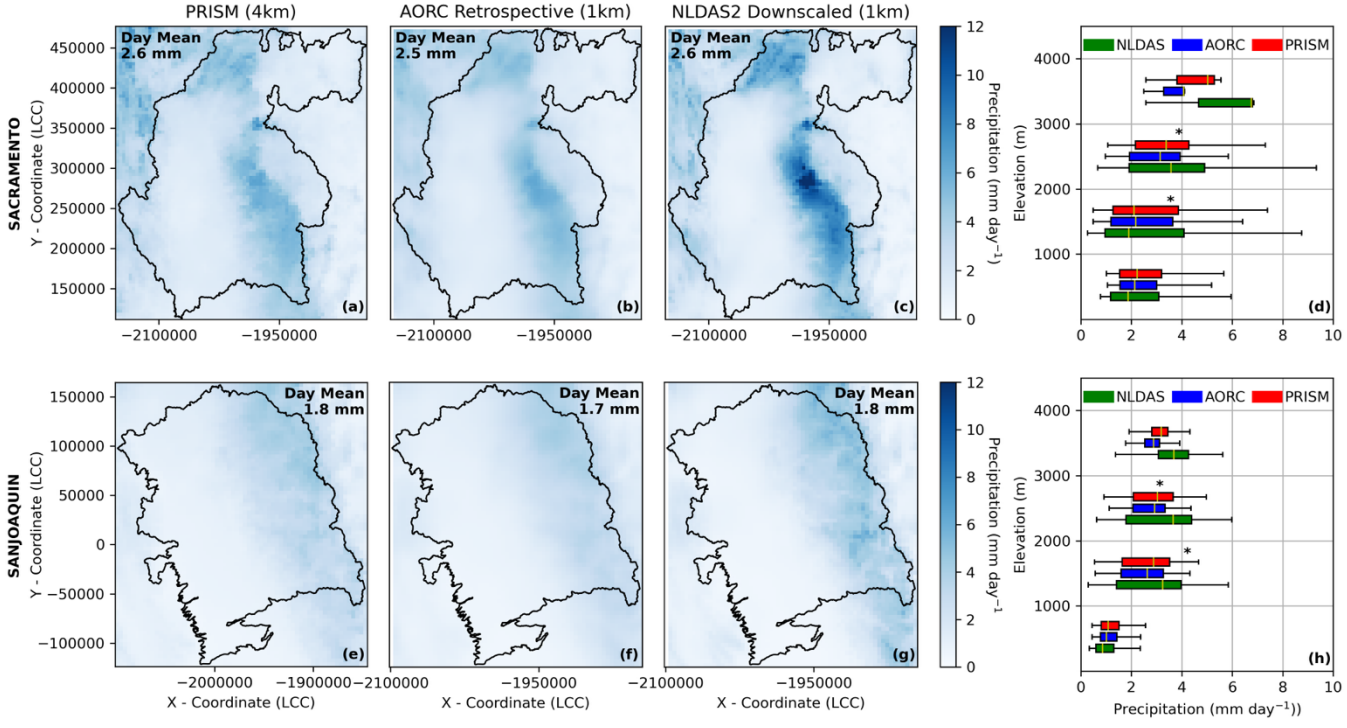


**Figure 2.** Downscaled 1 km AORC and NLDAS-2 precipitation (mm day$^{-1}$) compared to the 4 km PRISM data using WRF-Hydro MFE over the Sacramento (upper panel, a-c) and San Joaquin River Basins (lower panel, e-g). Spatial daily mean has been annotated in the plot. Boxplot of these gridded products over the two River Basins are plotted in d and h, * represents the mean from the available CDWR stations in each River Basins (Fig. 1).

The downscaled temperature from NLDAS-2 shows a higher temperature in valley regions and lower temperature in mountains regions compared to AORC and PRISM (Fig. 3). Having higher precipitation and lower temperature in NLDAS-2, makes suitable conditions for snow accumulation. In the Sacramento River Basin, the downscaled temperature can capture daily mean temperature compared to PRISM. The daily mean temperature of PRISM is 285.7ºK, whereas AORC and downscaled NLDAS-2 temperature are 285.4ºK (0.1ºK less) and 285.6ºK (0.3ºK less) respectively (Fig. 3a–c). The valley-mountain temperature difference is more noticeable in NLDAS-2 than AORC. Boxplots show that downscaled NLDAS-2 has colder temperatures compared to PRISM and AORC at higher elevations (>2000 m), with the reverse at lower elevations (<1000 m) (Fig. 3d). The available CDWR stations (represented with * in Fig. 3d, h) also closely follows the gridded datasets. In the San Joaquin River Basin, the daily-mean temperature of PRISM is 286.9 K, which is better captured by AORC. However, NLDAS-2 is higher by 0.6 K (Fig. 3e-g) and shows a stronger temperature gradient across the elevation gradient compared to the other two datasets. Like the Sacramento, Basin except the lower elevation (<2000 m), NLDAS-2 produces colder temperature compared to PRISM and AORC, and available CDWR stations shows the mean value in the boxplot range (Fig. 3h). The temperature downscaling based on the lapse rate provided by NCAR is sensitive to the altitudinal difference and thus causes the changes in the temperature gradient compared to PRISM.

https://doi.org/10.5194/egusphere-2025-3884
Preprint. Discussion started: 21 August 2025


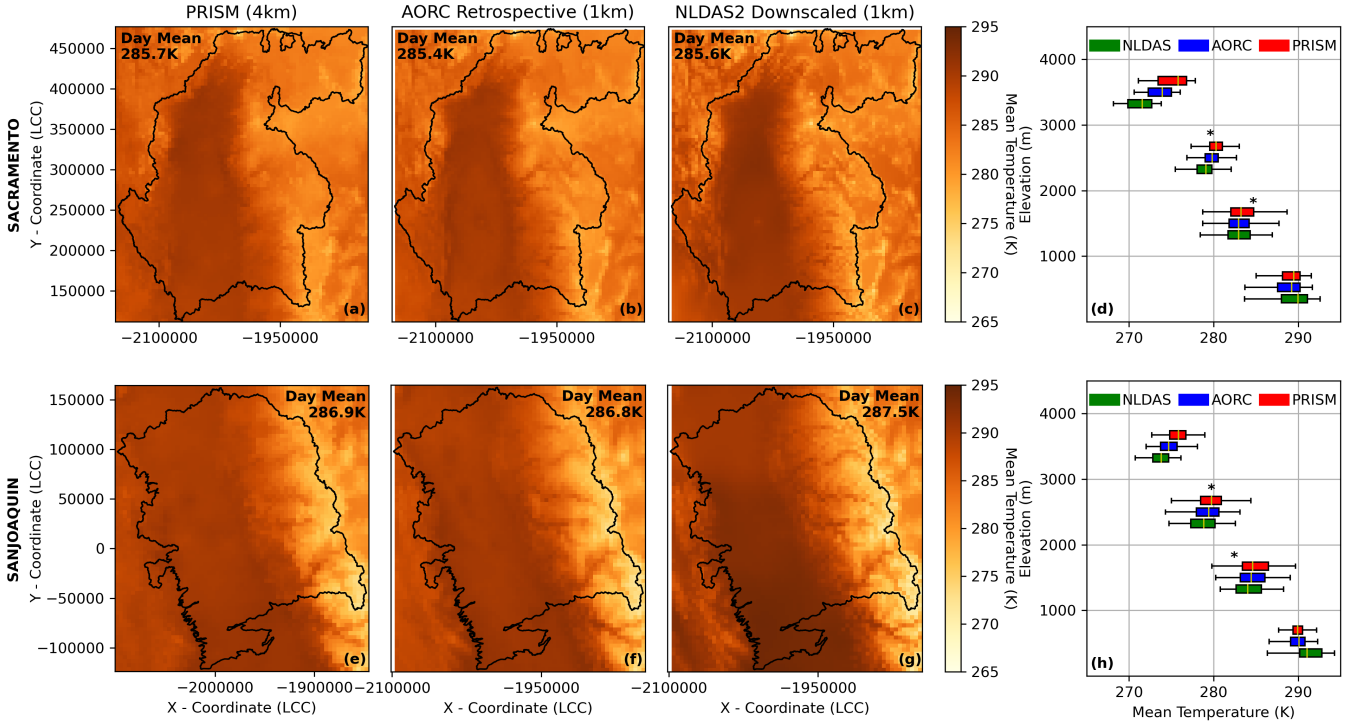


**Figure 3.** Downscaled 1km AORC and NLDAS-2 temperature compared to the 4 km PRISM data using WRF-Hydro MFE over the Sacramento (upper panel, a-c) and San Joaquin River Basins (lower panel, e-g). Daily mean averaged over the basins is annotated in the plot. Boxplot of these gridded products over the two River Basins are plotted in d and h, * represents the mean from the available CDWR stations in each River Basin (Fig. 1).

### 5.2 SWE sensitivity to Precipitation Forcing and dynamic Vegetation

We first analysed the sensitivity of the modeled SWE to different precipitation data and vegetation conditions (Fig. 4). In both river basins, the downscaled NLDAS-2 forcing produces more SWE than AORC forcing by up to 40 mm in the peak SWE. NLDAS-2 produces more SWE than SNODAS, whereas the AORC produces less SWE than SNODAS under all vegetation conditions. In all cases, the dynamic vegetation module results in less accumulated SWE than the default, prescribed vegetation by 20-25 mm. In the Sacramento (Fig. 4a & b), the impact of vegetation on the annual cycle of SWE is more notable than in the San Joaquin Basin (Fig. 4c & d) due to the less coverage of broadleaf and needleleaf forests in the San Joaquin compared to the Sacramento (Fig. 1). The dynamic vegetation module produces better results (closer to SNODAS) when driven by the NLDAS-2 forcing but worse when driven by AORC in both basins. These simulations suggest that the modeled SWE are most sensitive to the choice of precipitation products followed by the choice of vegetation schemes.

https://doi.org/10.5194/egusphere-2025-3884
Preprint. Discussion started: 21 August 2025


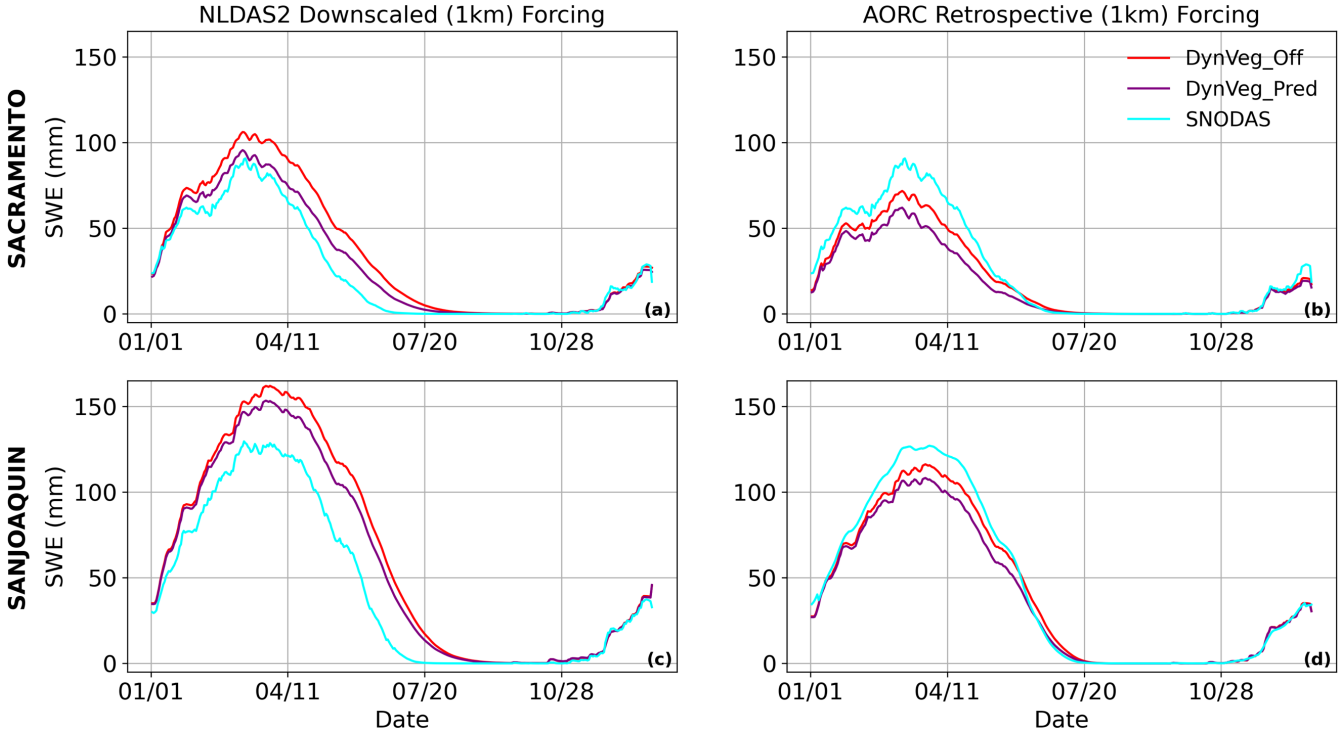


**Figure 4.** Modeled snow water equivalent (SWE) driven by different atmospheric forcing data (left panels: NLDAS-2; right panels: AORC) under the prescribed vegetation (DynVeg_Off) and dynamic vegetation (DynVeg_Pred) in the Sacramento (upper two panels) and San Joaquin (lower two panels) River Basins. Independent SWE estimates, SNODAS, is also included.

https://doi.org/10.5194/egusphere-2025-3884
Preprint. Discussion started: 21 August 2025


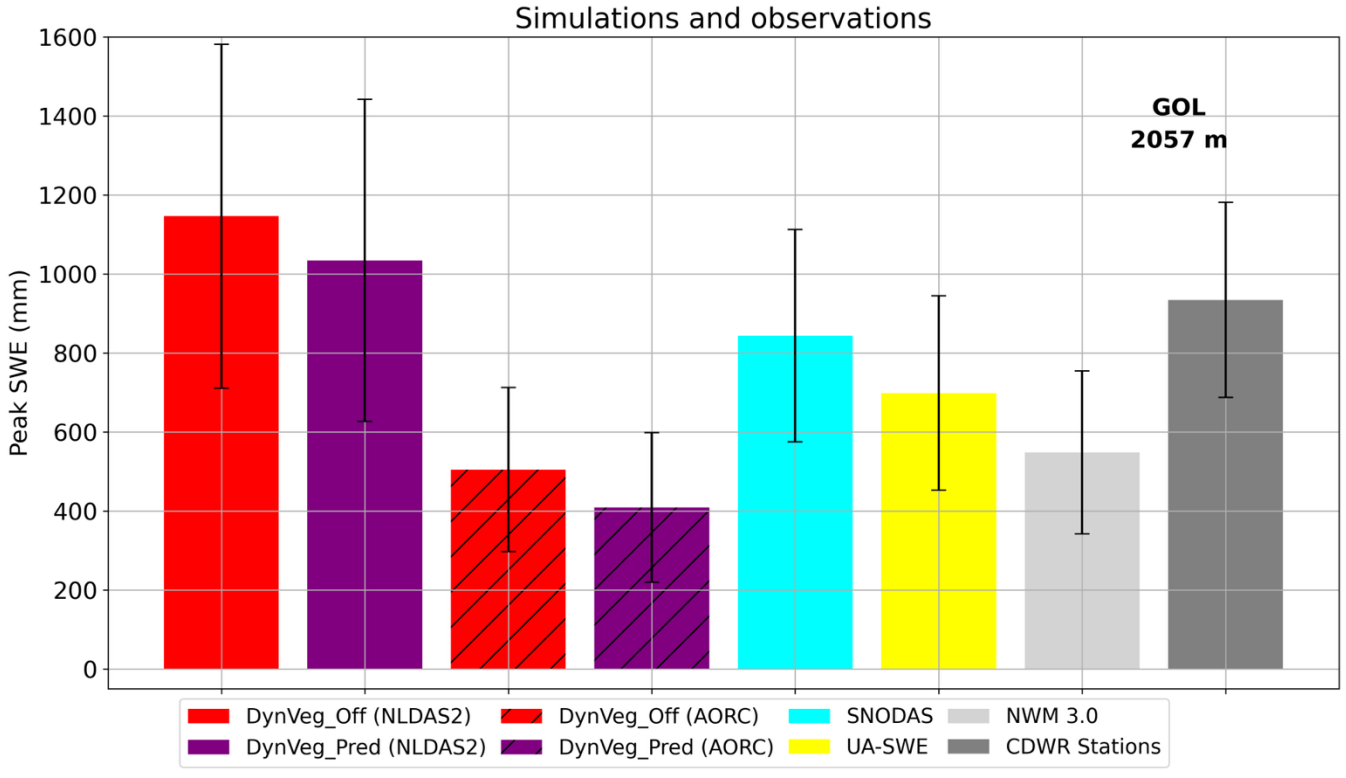


**Figure 5.** Snow water equivalent (SWE) comparison at a selected CDWR station (GOL, the Sacramento River Basin) out of the 23 stations. The modeled peak SWE (in March) driven by the NLDAS-2 and AORC (hatched bars) forcing are plotted against the gridded products (UA-SWE, SNODAS and NWM 3.0) and the CDWR stations (solid dark grey bar). The error bar represents the standard deviation from 11 Sacramento stations. The monthly SWE variation plot with all 23 stations is included in supplementary material (Fig. S1, Fig. S2).

We used 23 CDWR stations across the two river basins to evaluate the modeled SWE from different simulations. We show the results for all stations in the supplement (Fig. S1, Fig. S2), but here, we show the results from a single station (GOL) to illustrate the impact of forcing and dynamic vegetation on SWE simulation (Fig. 5). At this station, AORC produces less SWE when compared to CDWR (~300 mm during peak SWE) under both vegetation conditions. The simulation with NLDAS-2 and prescribed vegetation (DynVeg_Off) produce much larger SWE, which lasts longer (Fig. 5, Fig. S1, Fig. S2). The same simulation with dynamic vegetation (DynVeg_Pred) matches quite well with CDWR. The gridded SWE products also seem to be underestimated with SNODAS performing slightly better than UA-SWE and NWM 3.0. However, at a higher altitude the SWE difference becomes much larger. Here AORC simulations are underestimated by ~500 mm during the peak SWE period (Fig. S1, Fig. S2). The dynamic vegetation shortens the snow season compared to the simulation with prescribed LAI and matches well the observations. In general, except the GRM station (in the San Joaquin), NLDAS-2 forcing consistently produces better results (Fig. S1, Fig. S2). The higher elevation stations (CAP, GNL, TUM and HHM) shows that NLDAS-2 with dynamic vegetation produce optimum snow amount. At 11 CDWR stations in the Sacramento and 12 CDWR stations in

https://doi.org/10.5194/egusphere-2025-3884
Preprint. Discussion started: 21 August 2025


the San Joaquin, the model consistently performs better with NLDAS-2. This also supports daily SWE estimation in both river basins using NLDAS-2 (Fig. 4). The gridded UA-SWE and NWM 3.0 are underestimated, whereas SNODAS data are slightly better to match CDWR in terms of magnitude and seasonal cycle. The simulation with the prescribed vegetation shows a longer snow season than that of the gridded SNODAS data or CDWR. At the SLT, RBB, SNM, ADM, KIB, GOL, PSR, CAP and HRS stations, NLDAS-2 downscaled forcing produces SWE better than AORC forcing. In the lower altitude stations, NLDAS-2 SWE datasets are better than AORC, compared to CDWR. At the SLT, RBB, KIB, GOL, PSR, CAP and KSP stations, the simulations with the dynamic vegetation module capture the temporal variability better than its counterpart. Of particular interests, at the mid-altitude stations (HYS, GOL, PLP, PSR, CHM, BLD, TMR and SLM), there is a large difference between the simulations with and without the dynamic vegetation module because of the dominant broadleaf and needleleaf forests.

### 5.3 The Role of Vegetation Canopy

The difference between simulations with and without dynamic vegetation is the prediction of LAI. In both the river basins, the prescribed LAI (DynVeg_Off) is much higher than the predicted LAI (DynVeg_Pred) across almost all altitudes (Fig. 6). The prescribed LAI also shows less seasonality compared to the predicted LAI. The prescribed LAI values in DJF and MAM are higher than the MODIS LAI above 1000 m (Fig. 6 a–b). The simulations with the dynamic vegetation module produce LAI values closer to the MODIS LAI, especially in DJF at higher altitudes. Another independent LAI product from Sun Yat-sen University suggests slightly closer agreement with the dynamic vegetation simulation. The LAI values in DJF and MAM show that the dynamic vegetation model shows a capability of simulating the seasonal and altitudinal variability in LAI. Note that the prescribed LAI values (from Noah-MP parameters table) correspond to those used in NWM which affects the SWE dynamics in a similar manner (Johnson et al., 2023). The simulation driven by AORC produces slightly higher LAI compared to that by NLDAS-2 at higher altitudes (Fig. 6 c-d) due possibly to the warmer temperatures of AORC (Fig. 3d). The model predicted LAI can be further improved if the parameters controlling the leaf dynamics (e.g., the type-dependent specific leaf area, $m^2$/kg C) are further optimized.

https://doi.org/10.5194/egusphere-2025-3884
Preprint. Discussion started: 21 August 2025


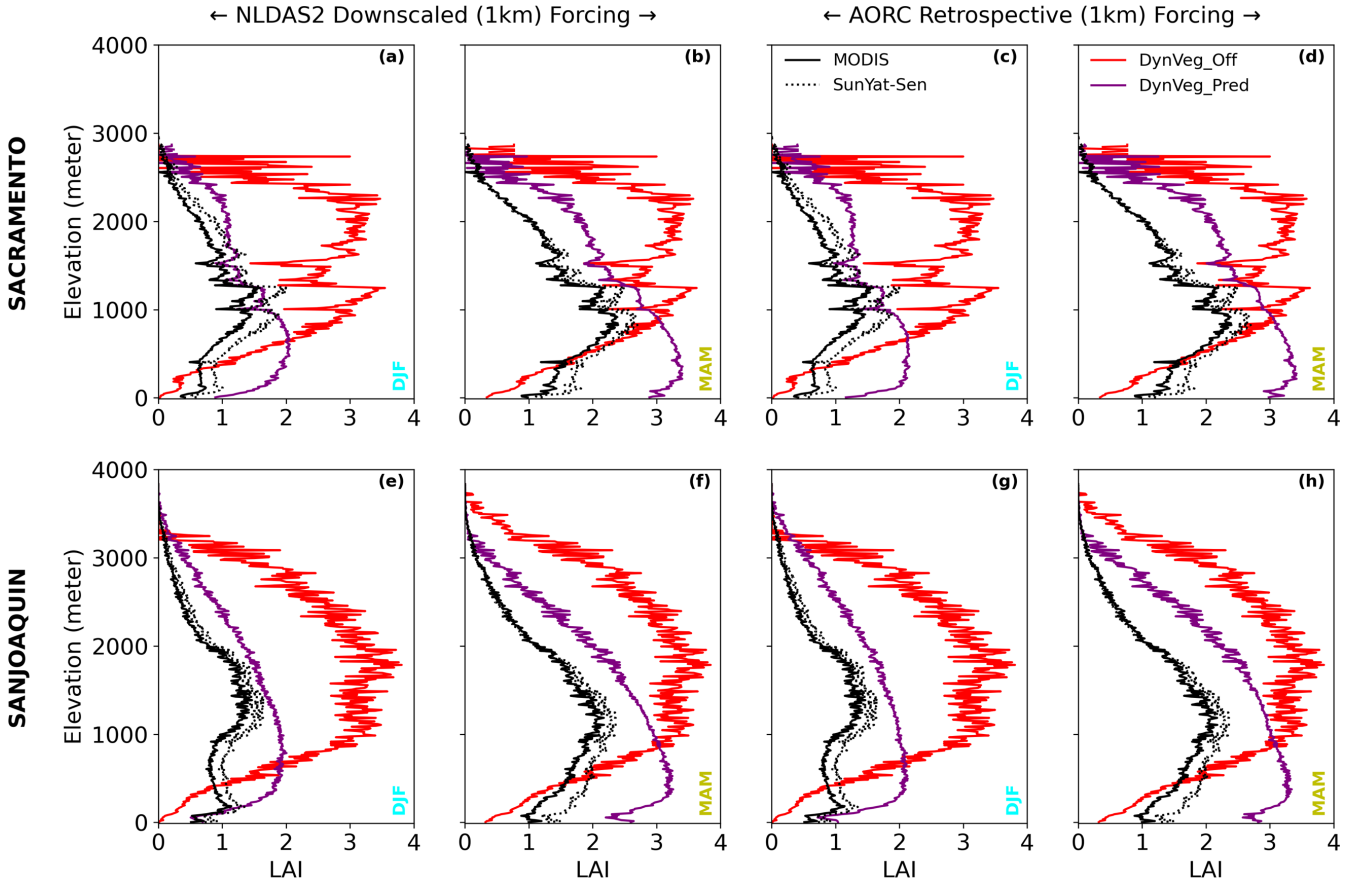


**Figure 6.** Altitudinal variation of the modeled leaf area index (LAI) for two seasons (winter: DJF, spring: MAM) using different atmospheric forcing data (two left panels: NLDAS-2; two right panels: AORC) under prescribed vegetation (DynVeg_Off) and dynamic vegetation (DynVeg_Pred) in the Sacramento (upper panel) and San Joaquin (lower panel) River Basins. Independent LAI estimates from the MODIS and Sun Yat-sen University are also included.

https://doi.org/10.5194/egusphere-2025-3884
Preprint. Discussion started: 21 August 2025


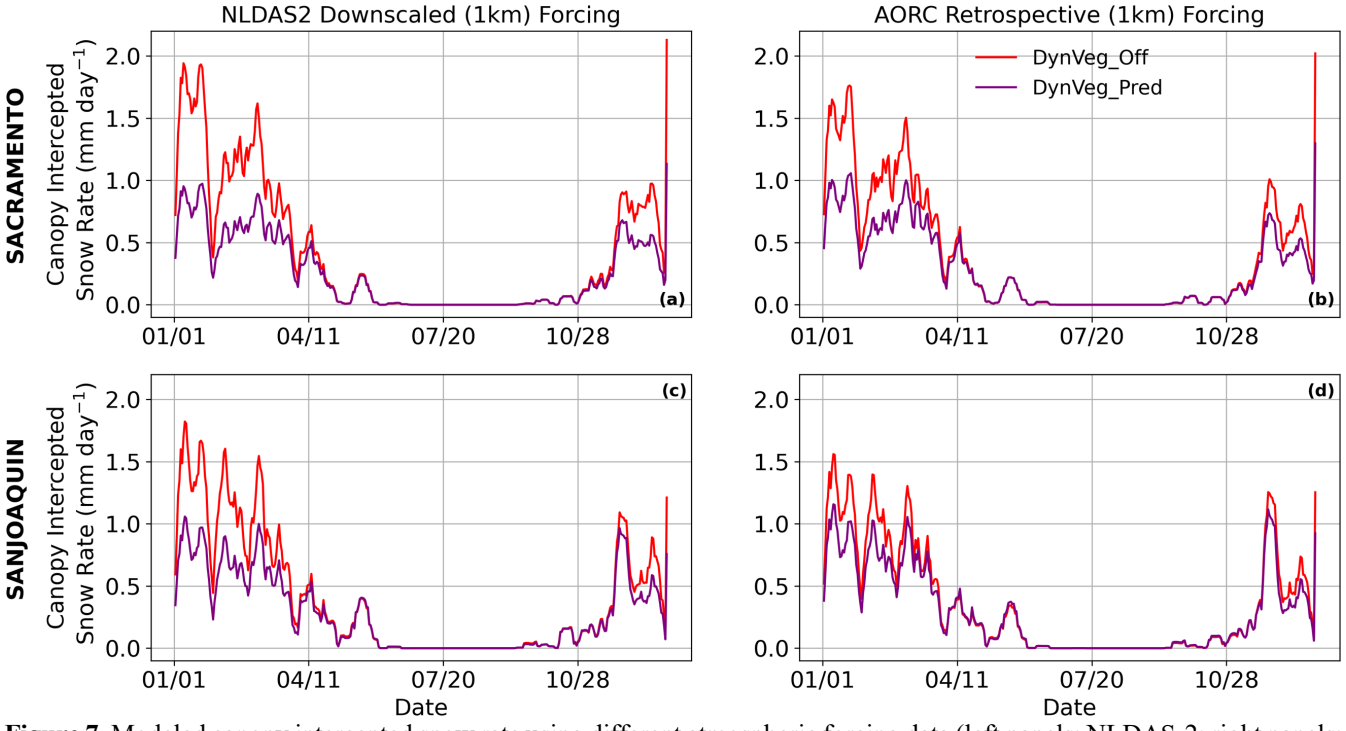


**Figure 7.** Modeled canopy intercepted snow rate using different atmospheric forcing data (left panels: NLDAS-2; right panels: AORC) under prescribed vegetation (DynVeg_Off) and dynamic vegetation (DynVeg_Pred) in the Sacramento (upper two panels) and San Joaquin (lower two panels) River Basins. A SWE threshold of 0.1 mm has been applied to mask the region.

Vegetation conditions directly impact the snow dynamics beneath the canopy through interception/sublimation of snow and changes in the energy budgets on the snow surface. The canopy intercepted snow resulting from DynVeg_Off is higher than DynVeg_Pred by up to 1.0 mm in both basins due to the larger prescribed LAI and GVF (Fig. S3 and S4) in DynVeg_Off (Fig. 7). The canopy intercepted snow is higher during the accumulation period and then decreases as snowfall decreases in the melting season. Driven by AORC, the canopy intercepted snow is smaller than that by NLDAS-2 (Fig. 7) due to the less snowfall (as a result of the less precipitation and warmer temperature) (Table 3). In the San Joaquin River, as the canopy density (LAI) is less than in the Sacramento, the differences in the canopy intercepted snow between the two experiments are less compared to the Sacramento River (Fig. 7c and d, Table 3). In general, the dynamic vegetation produces a lower ratio of canopy interception to actual snowfall, depending on LAI and vegetation cover fraction (GVF) (Table 3).

https://doi.org/10.5194/egusphere-2025-3884
Preprint. Discussion started: 21 August 2025


**Table 3**: Daily snowfall (SNOW) and daily canopy intercepted snow rate (ICEPT) for the different forcing datasets (NLDAS-2, AORC) under prescribed vegetation (DynVeg_Off) and dynamic vegetation (DynVeg_Pred) in Sacramento and San Joaquin River Basins. The table has been shown for the masked region similar to Figure 7.

| | | NLDAS-2 | | AORC | |
|---|---|---|---|---|---|
| | | DynVeg_Off | DynVeg_Pred | DynVeg_Off | DynVeg_Pred |
| SACRAMENTO (mm $d^{-1}$) | SNOW | 0.69 | 0.69 | 0.57 | 0.57 |
| | ICEPT | 0.41 | 0.25 | 0.38 | 0.27 |
| SANJOAQUIN (mm $d^{-1}$) | SNOW | 1.08 | 1.08 | 0.86 | 0.86 |
| | ICEPT | 0.39 | 0.27 | 0.34 | 0.28 |

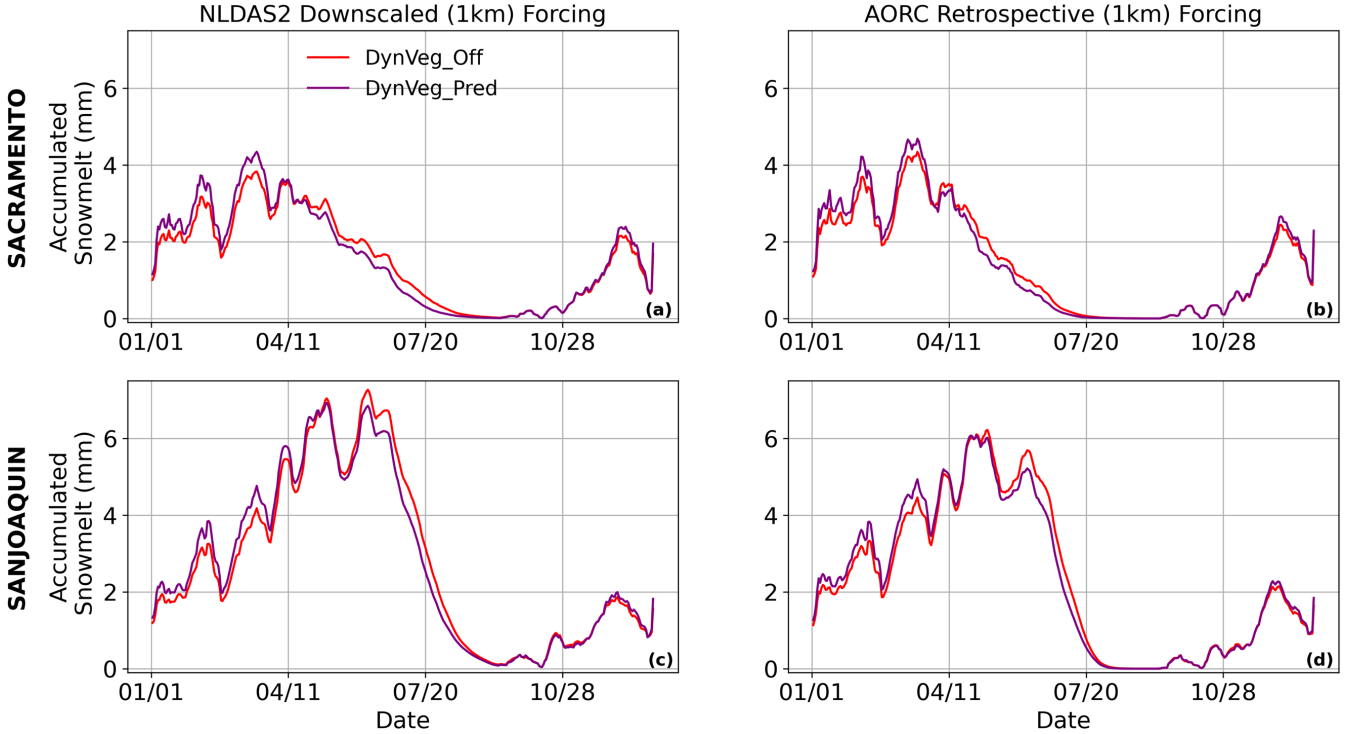


**Figure 8.** Modeled accumulated snowmelt rate using different atmospheric forcing data (left panels: NLDAS-2; right panels: AORC) under prescribed vegetation (DynVeg_Off) and dynamic vegetation (DynVeg_Pred) in the Sacramento (upper two panels) and San Joaquin (lower two panels) River Basins. A SWE threshold of 0.1 mm has been applied to mask the region.

https://doi.org/10.5194/egusphere-2025-3884
Preprint. Discussion started: 21 August 2025


The vegetation canopy with intercepted snow can substantially modify the energy budgets of the snow surface beneath the canopy and hence snowmelt (Fig. 8, Fig. S5). Unlike high-latitude regions, there are substantial episodic snowmelt occurring in the accumulation in these subtropical mountains. Driven by both forcing datasets (NLDAS-2 and AORC), the snowmelt rate in both river basins resulting from DynVeg_Off shows a lower melting rate by up to 0.5 mm day$^{-1}$ during the accumulation period (DJMF), resulting in the larger peak SWE resulting from DynVeg_Off (Fig. 4). Later in the melting the season (AMJJ), the snowmelt rate from DynVeg_Off exceeds that from DynVeg_Pred due mainly to the changes in solar radiation received by the snow surface (Figure 9; will be discussed later).

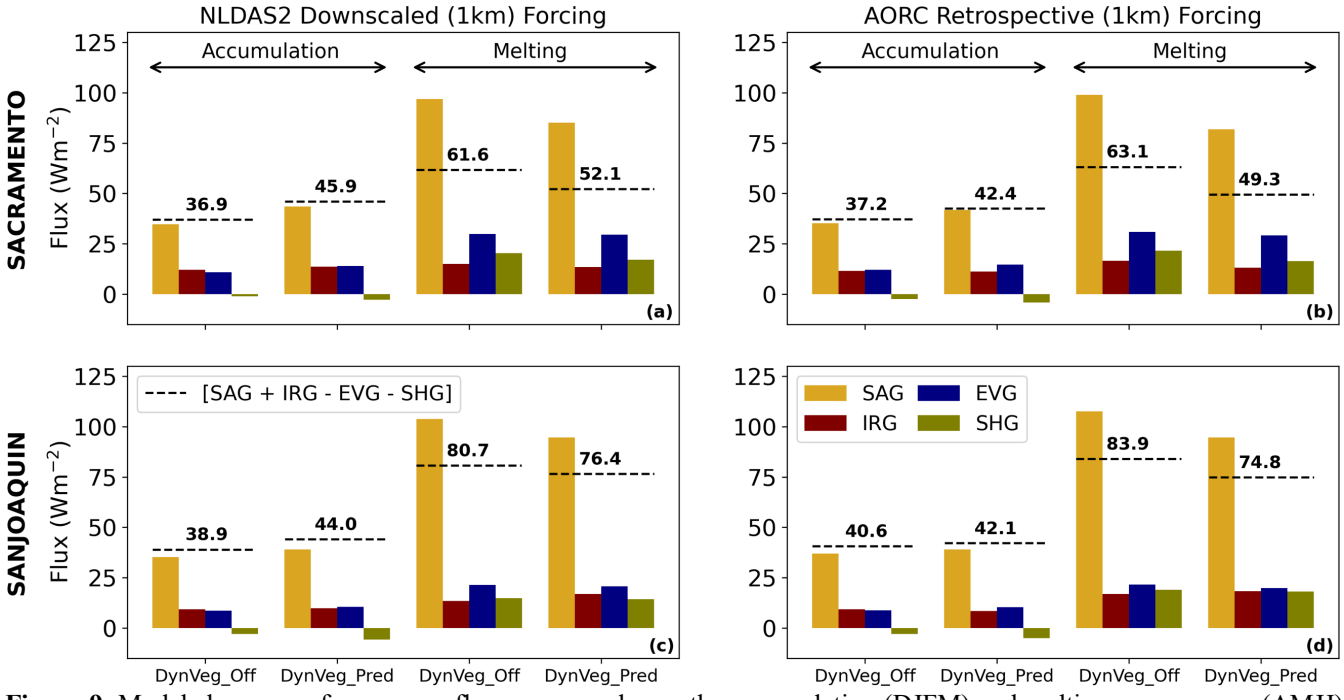


**Figure 9.** Modeled snow surface energy fluxes averaged over the accumulation (DJFM) and melting snow season (AMJJ) driven by different atmospheric forcing data (left panels: NLDAS-2; right panels: AORC) under prescribed vegetation (DynVeg_Off) and dynamic vegetation (DynVeg_Pred) in the Sacramento (upper two panels) and San Joaquin (lower two panels) River Basins. Acronyms correspond to net shortwave radiation (SAG), net longwave radiation (IRG), latent heat (EVG) and sensible heat (SHG) at the snow surface. The net budget is plotted as dashed lines and corresponding value is written on the top of the dashed lines. A SWE threshold of 0.1 mm has been applied to mask the region.

To disentangle the dominate control of snowmelt rate, we separately explored the below-canopy energy fluxes including the net shortwave radiation (SAG), net longwave radiation (IRG), latent heat (EVG) and sensible heat (SHG) fluxes at the snow surface during the accumulation (DJFM) and melting (AMJJ) seasons (Fig. 9). In Noah-MP, the energy available for snowmelt is controlled by the snow surface energy balance: SAG + IRG – EVG – SHG (Wm$^{-2}$). It turns out that the net solar radiation (received by the snow surface) is much larger than other energy balance components in all cases for both accumulation and meting season (Fig. 9). During the accumulation period (DJFM), the higher LAI in DynVeg_Off reduces the shortwave

https://doi.org/10.5194/egusphere-2025-3884
Preprint. Discussion started: 21 August 2025


radiation reaching the snow surface due mainly to the canopy shading effect, which is highly dependent on vegetation density (LAI and GVF) and solar angle. In the melting season (AMJJ), however, DynVeg_Off produces more snowmelt energy due mainly to the increasing LAI and GVF modeled by DynVeg_Pred (Fig. S3 & S4). GVF resulting from DynVeg_Pred exceeds that from DynVeg_Pred. The shading effect becomes more dependent on GVF than LAI when the solar elevation angle becomes larger (the Sun is more overhead). Other energy components also become larger in the melting season but the differences between the two experiments are much smaller compared to the shading effects.

## 6. Discussion

The AORC forcing is a well-known dataset for calibrating hydrological models over CONUS (Cosgrove et al., 2024; Kitzmiller et al., 2018). Over higher elevations (> 2,000 m), AORC underestimates precipitation than PRISM and NLDAS-2 (Fig. 2) but overestimate temperature than NLDAS-2, thereby producing less snowfall. Hence, the modelled SWE driven by AORC is significantly underestimated compared to the gridded estimates (UA-SWE and SNODAS) and more significantly when compared to the 23 CDWR stational data over the mountains. This is consistent with many other studies using the operational NWM, which adopts the same snow model of Noah-MP as used in this study and is driven by the same AORC forcing in the western United States (Garousi-Nejad and Tarboton, 2022; Yang et al., 2022, 2023).

The modeled SWE driven by NLDAS-2 produces much more SWE than by AORC. This is favourable when compared to the CDWR stational data but too much when compared to the gridded SWE products (SNODAS and UA-SWE). We compared the NLDAS-2 and AORC gridded precipitation to the CDWR stational precipitation (Fig. 10a & b). It seems that AORC matches better CDWR stations than does NLDAS-2 (Fig. 10a, b). However, the modeled SWE driven by AORC is much less than the observational SWE at the CDWR stations, whereas NLDAS-2 produces more comparable SWE (Fig. 10c and d). These conflicting results are mainly due to the fact that the CDWR precipitation data have not been corrected for gauge undercatch (Lundquist et al., 2015). When compared to the gridded SWE datasets, which are based on data assimilation (SNODAS) or machine learning (UA-SWE) using various in-situ SWE or snow depth measurements, the model driven by NLDAS-2 apparently overestimates SWE, but that driven by AORC definitely underestimate SWE. Considering that the CDWR stations may be preferred to be set up at sites with thicker snowpacks, which may result from deposition of wind-blown snow, the site-level CDWR measurements tend to overestimate SWE at the model grid scale (1 km). Considering the problem in the representativeness of these site-level CDWR measurements, NLDAS-2 with the prescribed vegetation (LAI and GVF) definitely overestimate SWE, but NLDAS-2 with the dynamic vegetation module produces more favourable SWE, which agrees better with the gridded SNODAS SWE. However, NLDAS-2 with the dynamic vegetation still produces more SWE than SNODAS, because the modeled LAI is still higher than the MODIS LAI.

https://doi.org/10.5194/egusphere-2025-3884
Preprint. Discussion started: 21 August 2025


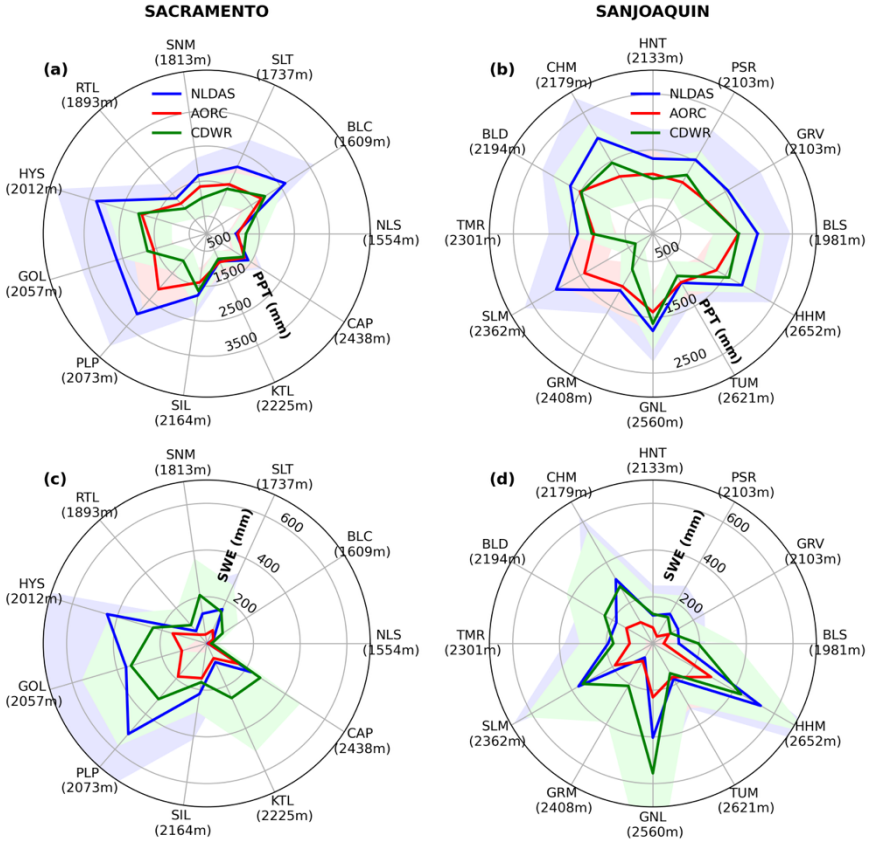


**Figure 10.** Comparison of yearly mean precipitation (a & b) and SWE (c & d) data from NLDAS-2 and AORC against the CDWR stational data (left panels: 11 stations in Sacramento River Basin; right panels: 12 stations in the San Joaquin River Basin). The modeled SWE data are taken from the DynVeg_Pred simulation. The shaded region represents the standard deviation of the datasets across 5 years at each station. The CDWR precipitation data are not corrected for gage undercatch.

## 7. Summary

Most hydrological models and LSMs, e.g., NWM (Garousi-Nejad and Tarboton, 2022), CLM (Toure et al., 2016), Noah-MP and other LSMs (Cho et al., 2022) significantly underestimate SWE, which is a major source of water to fill the surface reservoirs and recharge groundwater in the dry western US, and so do various global reanalyses like ERA, ERA-Land, MERRA-2 and GLDAS (Broxton, 2016). This modelling study in the Sacramento and San Joaquin River basins in California suggests that

1. The Noah-MP predicted SWE is most sensitive to the high-resolution (1 km) precipitation inputs. The use of the 1-km downscaled NLDAS-2 produces substantially more SWE than using AORC and NWM 3.0 (which also uses

https://doi.org/10.5194/egusphere-2025-3884
Preprint. Discussion started: 21 August 2025


AORC), especially at higher altitudes. This is favorable when compared to the CDWR stational data and other gridded products, e.g., SNODAS and UA SWE.

2. Following the precipitation inputs, the modeled SWE is also sensitive to the representations of vegetation dynamics. With the dynamic vegetation module, Noah-MP produces less SWE due mainly to the lower predicted LAI than the prescribed. This is favorable when the model is driven by the downscaled NLDAS-2 forcing. The lower predicted LAI may lead to less canopy interception of snowfall, resulting more SWE on the ground, but less significant shading effects, resulting in more shortwave radiation received by the snowpack beneath the canopy and thus more episodic snowmelt in the accumulation season. *The overall shading effect appears to be greater than the interception effects*, so the snowpack on the ground tends to be thinner and persist shorter when there is less vegetation canopies. The modeled LAI matches MODIS LAI better than does the prescribed but still higher than the MODIS LAI. Further calibration of vegetation parameters may result in lower LAI, which are preferable to produce less SWE and thus match the gridded SWE products (SNODAS and UA-SWE).

These findings highlight the importance of downscaling of atmospheric forcing and vegetation effects to the accuracy of snow modeling. Mountain mapper based NLDAS-2 downscaled data along with better representations of LAI and vegetation cover fraction can further improve snow predictions in the snow dominated river basins within NWM framework. The upcoming dynamically downscaled NLDAS-2 at 1 km resolution (i.e., NLDAS-3) is worth exploration for snow predictions in the western US.

**Code and data availability**

This study uses the open-source code and data. Noah-MP Version 5 is available at, https://github.com/NCAR/noahmp, the NLDAS-2 forcing data and MODIS LAI data can be dowloaded from, https://disc.gsfc.nasa.gov, PRISM data can be dowloaded from, https://prism.oregonstate.edu, AORC forcing and National Water Model (NWM) output data can be dowloaded from, https://noaa-nwm-retrospective-2-1-pds.s3.amazonaws.com/index.html. Details about the downscaling software can be found at, https://ral.ucar.edu/dataset/wrf-hydro-meteorological-forcing-engine-mfe-beta. Description about the observation snow data can be found from the California department of the Water Resource website, https://water.ca.gov. Sun Yat-Sen LAI data can be requested from, http://globalchange.bnu.edu.cn/research/data. SNODAS 1 km SWE data can be dowloaded from, https://nsidc.org/home, UA-SWE 1 km SWE data is available from personnel request from our co-author, Patrick Broxton and details can be found here, https://storymaps.arcgis.com.

https://doi.org/10.5194/egusphere-2025-3884
Preprint. Discussion started: 21 August 2025


**Acknowledgement**

This research was supported by the Cooperative Institute for Research to Operations in Hydrology (CIROH) with funding under award NA22NWS4320003 from the NOAA Cooperative Institute Program. The statements, findings, conclusions, and recommendations are those of the author(s) and do not necessarily reflect the opinions of NOAA.

**References**

Anderson, B. T., McNamara, J. P., Marshall, H., and Flores, A. N.: Insights into the physical processes controlling correlations between snow distribution and terrain properties, Water Resources Research, 50, 4545–4563, https://doi.org/10.1002/2013WR013714, 2014.

Ball, J. T., Woodrow, I. E., and Berry, J. A.: A Model Predicting Stomatal Conductance and its Contribution to the Control of Photosynthesis under Different Environmental Conditions, in: Progress in Photosynthesis Research, edited by: Biggins, J., Springer Netherlands, Dordrecht, 221–224, https://doi.org/10.1007/978-94-017-0519-6_48, 1987.

Barrett, A. P.: National Operational Hydrologic Remote Sensing Center Snow Data Assimilation System (SNODAS) Data Products at NSIDC, Version 1, https://doi.org/https://doi.org/10.7265/N5TB14TC, 2004.

Bartlett, P. A. and Verseghy, D. L.: Modified treatment of intercepted snow improves the simulated forest albedo in the Canadian Land Surface Scheme, Hydrol. Process., 29, 3208–3226, https://doi.org/10.1002/hyp.10431, 2015.

Bonan, G. B., Levis, S., Sitch, S., Vertenstein, M., and Oleson, K. W.: A dynamic global vegetation model for use with climate models: concepts and description of simulated vegetation dynamics, Global Change Biology, 9, 1543–1566, https://doi.org/10.1046/j.1365-2486.2003.00681.x, 2003.

Brekke, L. D., Miller, N. L., Bashford, K. E., Quinn, N. W. T., and Dracup, J. A.: CLIMATE CHANGE IMPACTS UNCERTAINTY FOR WATER RESOURCES IN THE SAN JOAQUIN RIVER BASIN, CALIFORNIA[1], J American Water Resour Assoc, 40, 149–164, https://doi.org/10.1111/j.1752-1688.2004.tb01016.x, 2004.

Broxton, P., Ehsani, M. R., and Behrangi, A.: Improving Mountain Snowpack Estimation Using Machine Learning With Sentinel-1, the Airborne Snow Observatory, and University of Arizona Snowpack Data, Earth and Space Science, 11, e2023EA002964, https://doi.org/10.1029/2023EA002964, 2024.

https://doi.org/10.5194/egusphere-2025-3884
Preprint. Discussion started: 21 August 2025


Chen, F., Barlage, M., Tewari, M., Rasmussen, R., Jin, J., Lettenmaier, D., Livneh, B., Lin, C., Miguez-Macho, G., Niu, G., Wen, L., and Yang, Z.: Modeling seasonal snowpack evolution in the complex terrain and forested Colorado Headwaters region: A model intercomparison study, JGR Atmospheres, 119, https://doi.org/10.1002/2014JD022167, 2014.

Collatz, G., Ribas-Carbo, M., and Berry, J.: Coupled Photosynthesis-Stomatal Conductance Model for Leaves of C4 Plants, Functional Plant Biol., 19, 519, https://doi.org/10.1071/PP9920519, 1992.

Collatz, G. J., Ball, J. T., Grivet, C., and Berry, J. A.: Physiological and environmental regulation of stomatal conductance, photosynthesis and transpiration: a model that includes a laminar boundary layer, Agricultural and Forest Meteorology, 54, 107–136, https://doi.org/10.1016/0168-1923(91)90002-8, 1991.

Cook, B. I., Bonan, G. B., Levis, S., and Epstein, H. E.: Rapid vegetation responses and feedbacks amplify climate model response to snow cover changes, Clim Dyn, 30, 391–406, https://doi.org/10.1007/s00382-007-0296-z, 2008.

Cooper, E. J., Dullinger, S., and Semenchuk, P.: Late snowmelt delays plant development and results in lower reproductive success in the High Arctic, Plant Science, 180, 157–167, https://doi.org/10.1016/j.plantsci.2010.09.005, 2011.

Cosgrove, B., Gochis, D., Flowers, T., Dugger, A., Ogden, F., Graziano, T., Clark, E., Cabell, R., Casiday, N., Cui, Z., Eicher, K., Fall, G., Feng, X., Fitzgerald, K., Frazier, N., George, C., Gibbs, R., Hernandez, L., Johnson, D., Jones, R., Karsten, L., Kefelegn, H., Kitzmiller, D., Lee, H., Liu, Y., Mashriqui, H., Mattern, D., McCluskey, A., McCreight, J. L., McDaniel, R., Midekisa, A., Newman, A., Pan, L., Pham, C., RafieeiNasab, A., Rasmussen, R., Read, L., Rezaeianzadeh, M., Salas, F., Sang, D., Sampson, K., Schneider, T., Shi, Q., Sood, G., Wood, A., Wu, W., Yates, D., Yu, W., and Zhang, Y.: NOAA's National Water Model: Advancing operational hydrology through continental-scale modeling, J American Water Resour Assoc, 60, 247–272, https://doi.org/10.1111/1752-1688.13184, 2024.

Daly, C., Taylor, G. H., Gibson, W. P., Parzybok, T. W., Johnson, G. L., and Pasteris, P. A.: HIGH-QUALITY SPATIAL CLIMATE DATA SETS FOR THE UNITED STATES AND BEYOND, Transactions of the ASAE, 43, 1957–1962, https://doi.org/10.13031/2013.3101, 2000a.

Daly, S. F., Davis, R., Ochs, E., and Pangburn, T.: An approach to spatially distributed snow modelling of the Sacramento and San Joaquin basins, California, Hydrol. Process., 14, 3257–3271, https://doi.org/10.1002/1099-1085(20001230)14:18<3257::AID-HYP199>3.0.CO;2-Z, 2000b.

Dickerson-Lange, S. E., Vano, J. A., Gersonde, R., and Lundquist, J. D.: Ranking Forest Effects on Snow Storage: A Decision Tool for Forest Management, Water Resources Research, 57, e2020WR027926, https://doi.org/10.1029/2020WR027926, 2021.

https://doi.org/10.5194/egusphere-2025-3884
Preprint. Discussion started: 21 August 2025


Dickinson, R. E., Shaikh, M., Bryant, R., and Graumlich, L.: Interactive Canopies for a Climate Model, J. Climate, 11, 2823–2836, https://doi.org/10.1175/1520-0442(1998)011<2823:ICFACM>2.0.CO;2, 1998.

Domagalski, J.: Occurrence and transport of total mercury and methyl mercury in the Sacramento River Basin, California, Journal of Geochemical Exploration, 64, 277–291, https://doi.org/10.1016/S0375-6742(98)00038-7, 1998.

Ek, M. B., Mitchell, K. E., Lin, Y., Rogers, E., Grunmann, P., Koren, V., Gayno, G., and Tarpley, J. D.: Implementation of Noah land surface model advances in the National Centers for Environmental Prediction operational mesoscale Eta model, J. Geophys. Res., 108, 2002JD003296, https://doi.org/10.1029/2002JD003296, 2003.

Ellis, C. R., Pomeroy, J. W., Essery, R. L. H., and Link, T. E.: Effects of needleleaf forest cover on radiation and snowmelt dynamics in the Canadian Rocky Mountains, Can. J. For. Res., 41, 608–620, https://doi.org/10.1139/X10-227, 2011.

Euskirchen, E. S., Bennett, A. P., Breen, A. L., Genet, H., Lindgren, M. A., Kurkowski, T. A., McGuire, A. D., and Rupp, T. S.: Consequences of changes in vegetation and snow cover for climate feedbacks in Alaska and northwest Canada, Environ. Res. Lett., 11, 105003, https://doi.org/10.1088/1748-9326/11/10/105003, 2016.

Fang, Y., Liu, Y., and Margulis, S. A.: A western United States snow reanalysis dataset over the Landsat era from water years 1985 to 2021, Sci Data, 9, 677, https://doi.org/10.1038/s41597-022-01768-7, 2022.

Farquhar, G. D., Von Caemmerer, S., and Berry, J. A.: A biochemical model of photosynthetic CO2 assimilation in leaves of C3 species, Planta, 149, 78–90, https://doi.org/10.1007/BF00386231, 1980.

Franklin, O., Harrison, S. P., Dewar, R., Farrior, C. E., Brännström, Å., Dieckmann, U., Pietsch, S., Falster, D., Cramer, W., Loreau, M., Wang, H., Mäkelä, A., Rebel, K. T., Meron, E., Schymanski, S. J., Rovenskaya, E., Stocker, B. D., Zaehle, S., Manzoni, S., Van Oijen, M., Wright, I. J., Ciais, P., Van Bodegom, P. M., Peñuelas, J., Hofhansl, F., Terrer, C., Soudzilovskaia, N. A., Midgley, G., and Prentice, I. C.: Organizing principles for vegetation dynamics, Nat. Plants, 6, 444–453, https://doi.org/10.1038/s41477-020-0655-x, 2020.

Garousi-Nejad, I. and Tarboton, D. G.: A comparison of National Water Model retrospective analysis snow outputs at snow telemetry sites across the Western United States, Hydrological Processes, 36, e14469, https://doi.org/10.1002/hyp.14469, 2022.

He, C., Valayamkunnath, P., Barlage, M., Chen, F., Gochis, D., Cabell, R., Schneider, T., Rasmussen, R., Niu, G.-Y., Yang, Z.-L., Niyogi, D., and Ek, M.: The Community Noah-MP Land Surface Modeling System Technical Description Version 5.0, UCAR/NCAR, https://doi.org/10.5065/EW8G-YR95, 2023.

https://doi.org/10.5194/egusphere-2025-3884
Preprint. Discussion started: 21 August 2025


Hedstrom, N. R. and Pomeroy, J. W.: Measurements and modelling of snow interception in the boreal forest, Hydrol. Process., 12, 1611–1625, https://doi.org/10.1002/(SICI)1099-1085(199808/09)12:10/11<1611::AID-HYP684>3.0.CO;2-4, 1998.

Hwang, T., Band, L., and Hales, T. C.: Ecosystem processes at the watershed scale: Extending optimality theory from plot to catchment, Water Resources Research, 45, 2009WR007775, https://doi.org/10.1029/2009WR007775, 2009.

Johnson, J. M., Fang, S., Sankarasubramanian, A., Rad, A. M., Kindl Da Cunha, L., Jennings, K. S., Clarke, K. C., Mazrooei, A., and Yeghiazarian, L.: Comprehensive Analysis of the NOAA National Water Model: A Call for Heterogeneous Formulations and Diagnostic Model Selection, JGR Atmospheres, 128, e2023JD038534, https://doi.org/10.1029/2023JD038534, 2023.

Jordan, R. E.: A One-dimensional temperature model for a snow cover : technical documentation for SNTHERM.89, 1991.

Kitzmiller, D. H., Wu, W., Zhang, Z., Patrick, N., and Tan, X.: The Analysis of Record for Calibration: A High-Resolution Precipitation and Surface Weather Dataset for the United States, in: AGU Fall Meeting Abstracts, H41H-06, 2018.

Lin, W., Yuan, H., Dong, W., Zhang, S., Liu, S., Wei, N., Lu, X., Wei, Z., Hu, Y., and Dai, Y.: Reprocessed MODIS Version 6.1 Leaf Area Index Dataset and Its Evaluation for Land Surface and Climate Modeling, Remote Sensing, 15, 1780, https://doi.org/10.3390/rs15071780, 2023.

Livensperger, C., Steltzer, H., Darrouzet-Nardi, A., Sullivan, P. F., Wallenstein, M., and Weintraub, M. N.: Earlier snowmelt and warming lead to earlier but not necessarily more plant growth, AoB PLANTS, 8, plw021, https://doi.org/10.1093/aobpla/plw021, 2016.

Lundquist, J. D., Abel, M. R., Henn, B., Gutmann, E. D., Livneh, B., Dozier, J., and Neiman, P.: High-Elevation Precipitation Patterns: Using Snow Measurements to Assess Daily Gridded Datasets across the Sierra Nevada, California*, Journal of Hydrometeorology, 16, 1773–1792, https://doi.org/10.1175/JHM-D-15-0019.1, 2015.

Moeser, D., Stähli, M., and Jonas, T.: Improved snow interception modeling using canopy parameters derived from airborne L i DAR data, Water Resources Research, 51, 5041–5059, https://doi.org/10.1002/2014WR016724, 2015.

Mott, R., Vionnet, V., and Grünewald, T.: The Seasonal Snow Cover Dynamics: Review on Wind-Driven Coupling Processes, Front. Earth Sci., 6, https://doi.org/10.3389/feart.2018.00197, 2018.

Myneni, R., Knyazikhin, Y., and Park, T.: MODIS/Terra Leaf Area Index/FPAR 8-Day L4 Global 500m SIN Grid V061, https://doi.org/10.5067/MODIS/MOD15A2H.061, 2021.

https://doi.org/10.5194/egusphere-2025-3884
Preprint. Discussion started: 21 August 2025


Niu, G. and Yang, Z.: Effects of vegetation canopy processes on snow surface energy and mass balances, J. Geophys. Res., 109, 2004JD004884, https://doi.org/10.1029/2004JD004884, 2004.

Niu, G.-Y., Yang, Z.-L., Mitchell, K. E., Chen, F., Ek, M. B., Barlage, M., Kumar, A., Manning, K., Niyogi, D., Rosero, E., Tewari, M., and Xia, Y.: The community Noah land surface model with multiparameterization options (Noah-MP): 1. Model description and evaluation with local-scale measurements, J. Geophys. Res., 116, D12109, https://doi.org/10.1029/2010JD015139, 2011.

O'Keefe, K., Bell, D. M., McCulloh, K. A., and Nippert, J. B.: Bridging the Flux Gap: Sap Flow Measurements Reveal Species-Specific Patterns of Water Use in a Tallgrass Prairie, JGR Biogeosciences, 125, e2019JG005446, https://doi.org/10.1029/2019JG005446, 2020.

Overgaard, J., Rosbjerg, D., and Butts, M. B.: Land-surface modelling in hydrological perspective – a review, Biogeosciences, 3, 229–241, https://doi.org/10.5194/bg-3-229-2006, 2006.

Petersky, R. S., Shoemaker, K. T., Weisberg, P. J., and Harpold, A. A.: The sensitivity of snow ephemerality to warming climate across an arid to montane vegetation gradient, Ecohydrology, 12, e2060, https://doi.org/10.1002/eco.2060, 2019.

Rey, D. M., Hinckley, E. S., Walvoord, M. A., and Singha, K.: Integrating observations and models to determine the effect of seasonally frozen ground on hydrologic partitioning in alpine hillslopes in the Colorado Rocky Mountains, USA, Hydrological Processes, 35, e14374, https://doi.org/10.1002/hyp.14374, 2021.

Roesch, A., Wild, M., Gilgen, H., and Ohmura, A.: A new snow cover fraction parametrization for the ECHAM4 GCM, Climate Dynamics, 17, 933–946, https://doi.org/10.1007/s003820100153, 2001.

Schmidt, R. A. and Gluns, D. R.: Snowfall interception on branches of three conifer species, Can. J. For. Res., 21, 1262–1269, https://doi.org/10.1139/x91-176, 1991.

Stähli, M., Jonas, T., and Gustafsson, D.: The role of snow interception in winter-time radiation processes of a coniferous sub-alpine forest, Hydrological Processes, 23, 2498–2512, https://doi.org/10.1002/hyp.7180, 2009.

Strasser, U., Warscher, M., and Liston, G. E.: Modeling Snow–Canopy Processes on an Idealized Mountain, Journal of Hydrometeorology, 12, 663–677, https://doi.org/10.1175/2011JHM1344.1, 2011.

Tennant, C. J., Harpold, A. A., Lohse, K. A., Godsey, S. E., Crosby, B. T., Larsen, L. G., Brooks, P. D., Van Kirk, R. W., and Glenn, N. F.: Regional sensitivities of seasonal snowpack to elevation, aspect, and vegetation cover in western N orth A merica, Water Resources Research, 53, 6908–6926, https://doi.org/10.1002/2016WR019374, 2017.

https://doi.org/10.5194/egusphere-2025-3884
Preprint. Discussion started: 21 August 2025


Wang, X., Wang, T., Guo, H., Liu, D., Zhao, Y., Zhang, T., Liu, Q., and Piao, S.: Disentangling the mechanisms behind winter snow impact on vegetation activity in northern ecosystems, Global Change Biology, 24, 1651–1662, https://doi.org/10.1111/gcb.13930, 2018.

Xia, Y., Mitchell, K., Ek, M., Sheffield, J., Cosgrove, B., Wood, E., Luo, L., Alonge, C., Wei, H., Meng, J., Livneh, B., Lettenmaier, D., Koren, V., Duan, Q., Mo, K., Fan, Y., and Mocko, D.: Continental-scale water and energy flux analysis and validation for the North American Land Data Assimilation System project phase 2 (NLDAS-2): 1. Intercomparison and application of model products, J. Geophys. Res., 117, 2011JD016048, https://doi.org/10.1029/2011JD016048, 2012.

Yang, K., Musselman, K. N., Rittger, K., Margulis, S. A., Painter, T. H., and Molotch, N. P.: Combining ground-based and remotely sensed snow data in a linear regression model for real-time estimation of snow water equivalent, Advances in Water Resources, 160, 104075, https://doi.org/10.1016/j.advwatres.2021.104075, 2022.

Yang, K., Rittger, K., Musselman, K. N., Bair, E. H., Dozier, J., Margulis, S. A., Painter, T. H., and Molotch, N. P.: Intercomparison of snow water equivalent products in the Sierra Nevada California using airborne snow observatory data and ground observations, Front. Earth Sci., 11, 1106621, https://doi.org/10.3389/feart.2023.1106621, 2023.

Yang, R. and Friedl, M. A.: Modeling the effects of three-dimensional vegetation structure on surface radiation and energy balance in boreal forests, J. Geophys. Res., 108, 2002JD003109, https://doi.org/10.1029/2002JD003109, 2003.

Yang, Z.-L., Niu, G.-Y., Mitchell, K. E., Chen, F., Ek, M. B., Barlage, M., Longuevergne, L., Manning, K., Niyogi, D., Tewari, M., and Xia, Y.: The community Noah land surface model with multiparameterization options (Noah-MP): 2. Evaluation over global river basins, J. Geophys. Res., 116, D12110, https://doi.org/10.1029/2010JD015140, 2011.